it is this which was called the peak. Shifts on the order of the binding energy would have resulted in a Compton shift of 0.0401 Å, which is clearly not indicated by these studies.

[1]J. W. H. Dumond, Phys. Rev. 33, B643 (1929).
[2]W. Phillips and R. J. Weiss, Phys. Rev. 171, 790 (1968).
[3]M. Cooper and J. A. Leake, Phil. Mag. 15, 1201 (1967).
[4]R. J. Weiss and W. Phillips, Phys. Rev. 176, 900 (1968).
[5]A. Theodassious and P. Vosnidis, Phys. Rev. 145, B458 (1966).
[6]R. J. Weiss, Phys. Rev. Letters 24, 883 (1970).
[7]J. W. H. Dumond and H. A. Kirkpatrick, Phys. Rev. 52, 419 (1937).
[8]P. Eisenberger and P. Platzman, Phys. Rev. A 2, 415 (1970).
[9]B. Henneker (private communication).
[10]W. A. Rachinger, J. Sci. Instr. 25, 254 (1968).
[11]A. R. Stokes, Proc. Phys. Soc. (London) 61, 382 (1948).
[12]E. Clementi, IBM J. Res. Develop. Suppl. 9, 2 (1965).
[13]N. Sabelli and J. Hinze, J. Chem. Phys. 50, 648 (1969).
[14]P. Cade (private communication).
[15]A. C. Wahl and G. Das, J. Chem. Phys. 44, 87 (1966).
[16]D. Chip and L. O. Jennings, Phys. Rev. 132, B728 (1963).
[17]E. O. Wollan, Phys. Rev. 37, 862 (1931).
[18]F. Bloch, Phys. Rev. 45, 674 (1934).
[19]P. Kirkpatrick and P. A. Ross, Phys. Rev. 45, 667 (1934).

PHYSICAL REVIEW A VOLUME 2, NUMBER 5 NOVEMBER 1970

Ion Excitation of Characteristic X Rays for Elements with $72 \leqslant Z \leqslant 92$

P. B. Needham, Jr. and B. D. Sartwell
College Park Metallurgy Research Center, Bureau of Mines,
U. S. Department of the Interior, College Park, Maryland 20740

A systematic study has been made of the ionization cross sections for ion excitation of the M-shell x rays of elements with Z in the region $72 \leq Z \leq 92$. Protons, H_2^+ ions, and α particles with incident energies ranging from 60 to 400 keV were used to excite the M lines of Hf, Ta, W, Au, Bi, and U. The Z dependence of the proton-excited x-ray yield for these elements, although differing sharply from previously published M-shell results, is shown to be consistent with the Z dependence for proton excitation of the K and L shells reported in earlier papers. Finally, we have compared the ionization cross sections of H_2^+ ions at incident energy E_0 with those for protons at incident energy $\frac{1}{2}E_0$, and found that within 30% they are in the ratio 2:1.

INTRODUCTION

The excitation of characteristic x rays from many solid materials by the impact of energetic ions has been extensively studied in recent years.[1-6] Previous publications have reported quite extensively on the K shells of low-Z elements and L shells of medium-Z elements, but little work has been reported on the excitation of M-shell x rays. Theoretical work has been restricted principally to calculation of K-shell and, to a lesser extent, L-shell ionization cross sections. The purpose of this paper is to present a systematic experimental study of the M-shell excitation of elements with $72 \leq Z \leq 92$ under bombardment by H^+, H_2^+, and He^{++} ions in the energy range 60–400 keV.

The calculations of the K-shell ionization cross sections by Henneberg[7] and Huus,[8] and later by Merzbacher and Lewis,[9] remain as the principal theoretical works. These calculations utilized a Bethe-Born approximation, using plane wave functions for the incident projectile and unperturbed atomic wave functions for the electrons to be ejected from the target atom during the collision process. The failure of this approach for protons at low (< 200 keV) energies resulted in the use of relativistic wave functions for the K-shell electrons by Jamnik and Zupancic.[10] The relativistic corrections proved to be significant only for high-Z elements and still failed to provide good agreement with experimental measurements. A semiclassical time-dependent perturbation method was used by Bang and Hansteen,[11] in which the deflection of the projectile in the Coulomb field of the nucleus of the target atom was shown to be significant for projectiles incident at low energies. However, these corrections failed to match known experimental results for protons below 150 keV.

Recently, Brandt *et al.*[12] considered the effects of the binding of the K electrons of the target atom to the incident ion as a perturbation to the normal-shell binding energy. Specifically in the case of 25–250-keV protons and α particles on aluminum, the inclusion of this "binding effect" has provided excellent agreement between theory and experiment.

In the present paper, we have measured the ionization cross sections for M-shell excitation of Hf, Ta, W, Au, Bi, and U by impact of H^+, H_2^+, and He^{++} ions in the 60–400-keV energy range. The systematics of our results differ sharply from the few published results currently available. We feel that these differences are due to our use of more accurate values for the stopping power of the ions, fluorescence yields, and improved surface conditions of the targets. We also discuss the yields obtained with H_2^+ ions after impact dissociation occurs and show that the cross sections are approximately twice those for protons at one-half the incident energy.

EXPERIMENTAL WORK

Components of the experimental apparatus include an rf excited-ion source, 19-electrode accelerator column, beam analysis and collimation, target suppression, x-ray detection, and counting systems.

The ion source, accelerator column, and analyzing magnet are part of an A. I. 300-kV ion-accelerator facility located at the U. S. Bureau of Mines, College Park Metallurgy Research Center, College Park, Md. The hydrogen and helium used in the ion source were high-purity research-grade gases. Energy calibration of the ion beam from the accelerator was accomplished by using a precision resistor string with which the accelerating-column voltage was determined to an accuracy of 1%. In addition, the $B^{11}(p, \gamma)C^{12}$ resonance at a proton energy of 163 keV was utilized.

Prior to entering the analyzing magnet, the beam was focused by a strong-focusing quadrupole lens to approximately 6 mm in diameter on the 3-mm entrance slit to the magnet chamber. The radius of curvature of the analyzing magnet is 40.6 cm with a maximum field strength of 10 kG.

Collimation for the analyzed beam consisted of two 4-mm apertures, 0.85 m apart, with the second aperture located at the entrance to the target chamber. The target chamber is shown in Fig. 1 (a) and the target holder and secondary-electron suppression apparatus are shown in Fig. 1 (b). A 4-mm collimator [Fig. 1 (b)] maintained at positive 300 V was located in front of the secondary-electron shield to prevent any electrons produced by ions scattering from the walls of the beam tube from reaching the target. The diameter of the entrance hole of the secondary-electron shield was 6 mm to prevent the 4-mm beam from glancing off the edge of the shield and producing electrons that would strike the target. The secondary-electron shield was maintained at 150 V negative with respect to the target to provide for the suppression of secondary electrons from the target. Target current was measured using a current digitizer, the output of which was fed into a preset scalar. The preset scalar gated the input of a multichannel pulse-height analyzer, providing for preselection of the amount of charge to be accumulated on the target. The integrated dose was kept below 10^{14} ions/cm^2 to minimize effects caused by radiation damage.

An alternate method for suppressing secondary electrons was also used. This method, first described by Khan *et al.*,[5] used positive-target and secondary-electron shield voltages. A careful comparison showed that target-current measurements for each arrangement differed by less than 5% for the ion-beam energy range used here.

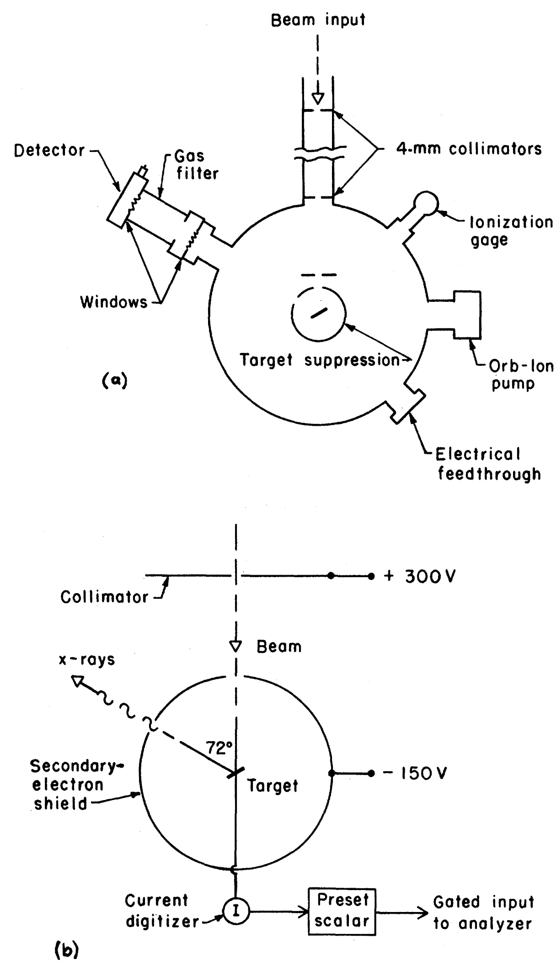

FIG. 1. (a) Target chamber used for heavy-ion production of x rays showing the final beam collimation, target suppression, thin Mylar windows, gas filter, and gas-flow detector. (b) Expanded view of the target secondary-electron suppression apparatus.

TABLE I. Values used for the detector quantum efficiency (QE), inner Mylar-window transmission (T_1), and aluminized Mylar-detector-window transmission (T_2) are given as a function of x-ray wavelength. The detector was operated with P-10 gas at atmospheric pressure, and the windows were 3.93 μ and 2.0 μ, respectively. The detector subtended a solid angle of 4.01×10^{-3} sr.

λ (Å)	T_1 (%)	T_2 (%)	QE (%)
3.91 (U)	95	98	52
5.12 (Bi)	87	94	77
5.84 (Au)	82	90	90
6.98 (W)	71	84	100
7.25 (Ta)	69	82	100
7.54 (Hf)	67	80	100

The ion beam was incident on the target an an angle of 36° to the target normal, and the detector was placed at an angle of 72° with respect to the incident-beam direction. The x rays produced in the target first passed through a 3.9-μ Mylar window into a gas-absorption x-ray filter. By admitting different gases into the filter at controlled partial pressures, x-ray wavelengths that might interfere with the primary wavelength to be studied could be eliminated. However, in the present experiment the filter was not utilized as an absorption chamber and was maintained at a vacuum of 10^{-3} Torr. The x-rays then passed through a 2-μ aluminized Mylar window into a gas-flow proportional counter. The detector had dimensions of 1.6-in. diam and 3.9-in. length, with a center wire 0.0025-in. diam. The counter gas was 90% argon-10% methane at atmospheric pressure. The quantum efficiency (Table I) for the detector at the different wavelengths was obtained from a plot of quantum efficiency versus wavelength given in the manufacturer's specifications. The transmission as a function of wavelength for each window used in either the gas-absorption filter or the gas-flow detector was calibrated prior to being used. The transmission at each wavelength was periodically remeasured to correct for stretching of the windows due to any large differential pressures (see Table I).

The signal from the detector was amplified and fed into both a single-channel analyzer and the ND-2200 pulse-height analyzer. The count rate was monitored by scalar-timers connected to the single-channel analyzer, and the integrated peaks were obtained from the spectra accumulated in the multichannel analyzer. The analyzer was inhibited by a preset scalar after a preselected amount of charge had been accumulated on the target.

The ultrahigh-purity (99.999%) targets were mechanically polished, chemically etched, rinsed with distilled water, dried in a blast of dry nitrogen, and then heated *in vacuo* at 200 °C for 10 min. Target contamination was kept at a minimum by maintaining a vacuum of 5×10^{-7} Torr in the beam line and $<8\times10^{-8}$ Torr in the target chamber during the experiment. The target chamber was pumped by a 4-in. orb-ion pumping system and, with no beam into the target chamber, a residual background pressure of 5×10^{-9} Torr was maintained.

EXPERIMENTAL RESULTS

The x-ray production cross sections σ_x were calculated from the standard equation for the x-ray production cross section[9]

$$\sigma_x = \frac{1}{\rho N}\frac{dI_\mu}{dE}\frac{dE}{dx} + \frac{1}{N}\frac{\mu}{\rho} I_\mu , \qquad (1)$$

where N = number of atoms per g, $-dE/dx$ = stopping power in keV/g cm^{-2}, μ/ρ = self-absorption of the target for its own x rays, I_μ = x-ray yield in photons/ion, and dI_μ/dE = the slope of the experimental-yield-versus-energy curve.

The x-ray production cross section σ_x is related to the ionization cross section σ_I as

$$\sigma_I = (1/\overline{\omega}_m)\sigma_x , \qquad (2)$$

where $\overline{\omega}_m$ is the average fluorescence yield of the mth atomic shell.

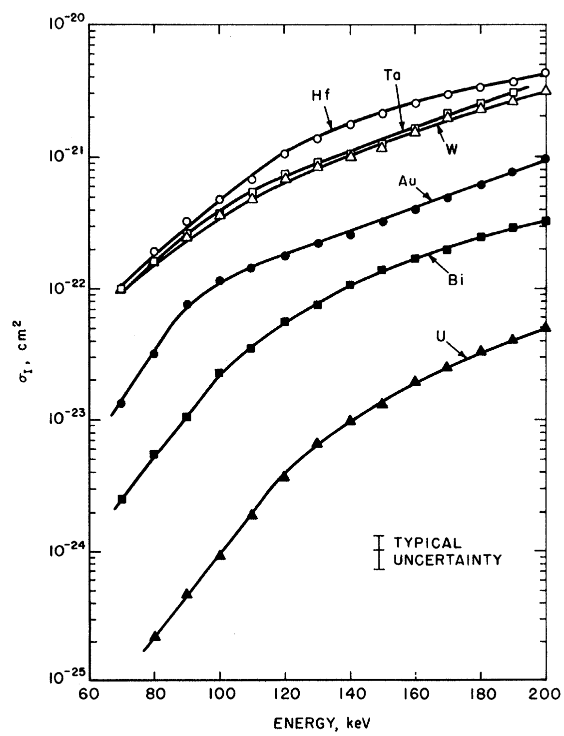

FIG. 2. The ionization cross sections for the M shells of Hf, Ta, W, Au, Bi, and U excited by protons are plotted as a function of incident proton energy in keV. The typical uncertainty in this figure and Figs. 3–6 is due principally to uncertainties in values used for the fluorescence yield $\overline{\omega}_m$, and stopping power $S(E)$.

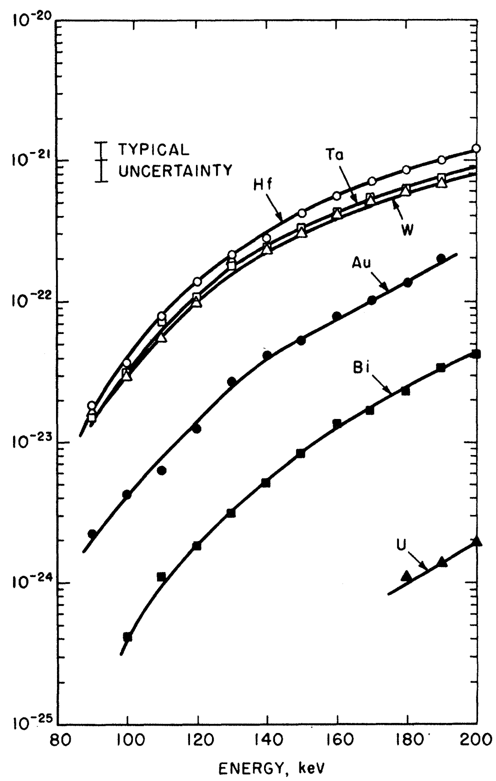

FIG. 3. Ionization cross sections for the M shells of Hf, Ta, W, Au, Bi, and U excited by H_2^+ ions are plotted as a function of incident-ion energy.

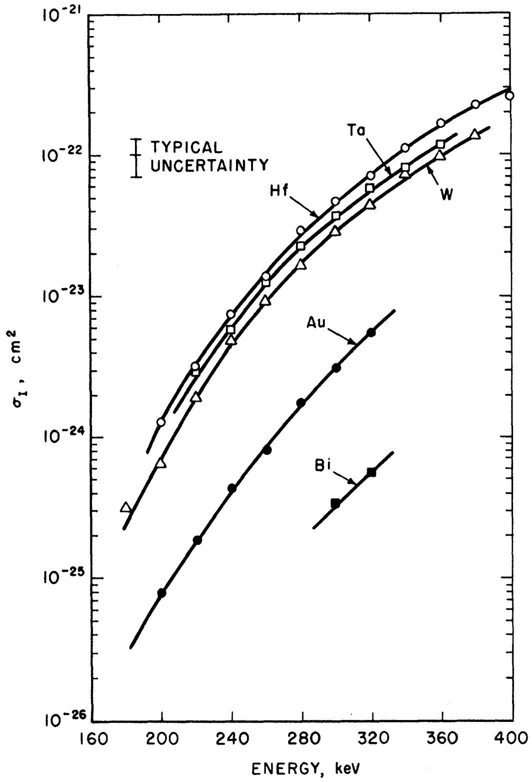

FIG. 4. Ionization cross sections for the M shells of Hf, Ta, W, Au, and Bi excited by He^{++} ions are plotted as a function of incident-ion energy.

The ionization cross sections obtained for H^+, H_2^+, and He^{++} ions are shown in Figs. 2–4. Complete tables with the detailed calculations are available from NAPS. Each value for the experimentally determined x-ray yield I_μ used in the calculation of the x-ray production cross section σ_x is the mean of three sets of data runs, each of which was independently run after a separate sequence of target polishing, mounting, and bakeout. This was done in order to average out any effects caused by surface preparation, contamination, and mounting geometry. The uncertainty in these measurements was less than 10%. However, the total uncertainty in the cross sections σ_I is estimated to be 30%. This is due principally to the uncertainty in the values of the stopping powers and fluorescence yields used in the calculation of Eqs. (1) and (2). The values for μ/ρ were taken from Champion *et al.*[13] Values of $\bar{\omega}_m$ are a result of interpolation or extrapolation of the few published values available.[14] The stopping powers we have utilized are mostly a result of interpolation. The values of $S(E)$ for H^+ were obtained from Warshaw and Allison,[15] and the values for He^{++} were obtained from Northcliffe.[16] The interpolated values of $S(E)$ for H_2^+ are the least reliable, since they were estimated by using stopping-power-versus-Z curves for ions of equal velocities obtained from a paper by Steward and Wallace.[17] Some measure of the accuracy of the values of $S(E)$ for H_2^+ ions can be obtained from a comparison of the cross sections σ_I for the H_2^+ ions, with incident energy E_0, with σ_I for H^+ ions, with incident energy $\frac{1}{2}E_0$, if the assumption is made that upon impact the H_2^+ ion dissociates with the kinetic energy divided equally between the two resulting hydrogen ions. We would expect, on this basis, the observed cross sections to have the ratio

$$\sigma_I^{H_2^+}[E_0] = 2\sigma_I^{H^+}[\tfrac{1}{2}E_0]. \tag{3}$$

Table II contains the results for the ratios for sev-

TABLE II. Ratios $\sigma_I(H_2^+)/\sigma_I(H^+)$ of the experimentally determined ionization cross sections for H_2^+ with incident energy E_0 and H^+ with incident energy $\frac{1}{2}E_0$. Each value for R is the mean value of the ratios for values of E_0=100, 120, 150, 180, and 200 keV.

Target	$R=\sigma_I(H_2^+)/\sigma_I(H^+)$
Hf	2.78 ± 0.25
Ta	2.44 ± 0.25
W	2.22 ± 0.69
Au	2.45 ± 0.29
Bi	2.14 ± 0.19
U	2.28 ± 0.14

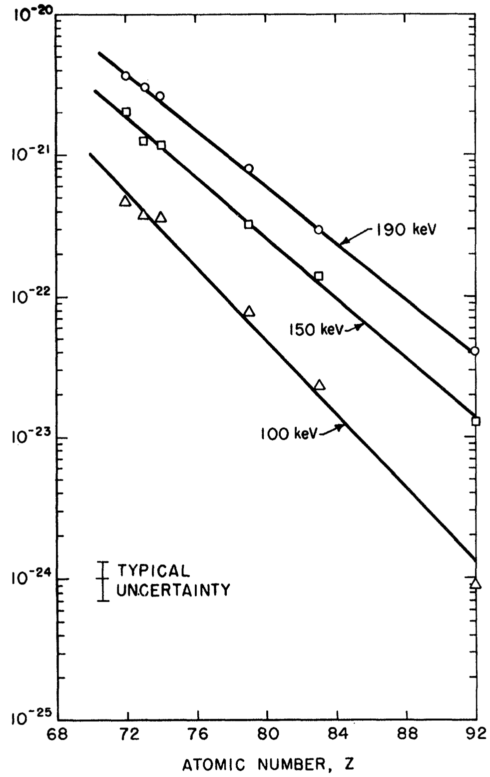

FIG. 5. M-shell ionization cross sections as a function of target atomic number Z for 100- , 150- , and 190-keV incident protons.

eral target materials. Each ratio is an average of the ratios at several incident-particle energies. The agreement with Eq. (3) is reasonably good and indicates that the estimated values of $S(E)$ for the H_2^+ ions were good within ca. 50%.

Only a few data points for uranium are shown in Fig. 3 for the H_2^+ ions in order to avoid using data which resulted from accumulation of large ion doses on the target. This would be necessary for the targets with highest Z where the x-ray yields have fallen off several orders of magnitude at the lowest incident-ion energies. Similarly, only two data points are utilized in Fig. 4 for α particles incident on bismuth, and no data for uranium are presented. The variation of the ionization cross section σ_I with target atomic number Z is shown for protons at 100, 150, and 190 keV in Fig. 5. Figure 6 shows σ_I versus Z for H^+ and H_2^+ ions incident at 190 keV and for He^{++} ions at 220 keV.

In Fig. 7 we have plotted the systematics for the x-ray yield I_μ as a function of the target atomic number Z for protons incident at 100 keV. We have included earlier data obtained by Khan *et al.*,[18] as well as the x-ray yield obtained for the Rh M line in another experiment performed by the authors. The x-ray yield I_μ has been plotted instead of the cross section σ_I in order to remove large variations possible in choices of the fluorescence yields $\bar{\omega}_m$, self-absorption μ/ρ, and stopping power $S(E)$.

It is immediately apparent that the earlier data obtained by Khan *et al.*[18] exhibit systematics sharply different from the data of this experiment for Z less than 70. An extrapolation of the curve through Khan's data points in Fig. 7 would indicate for the Rh M shell an x-ray yield more than 2 orders of magnitude below our value $I_\mu = 9.5\times10^{-5}$ photons/proton. A factor that might affect the rhodium yield would be a contribution from the carbon K line (44.5 Å) due to contamination in the form of CO on our target surface. For the Rh M shell it is the $M_{\mathrm{IV,V}}N_{\mathrm{II,III}}$ (47.67-Å) transition which is observed, and, with nondispersive x-ray analysis, it is not possible to resolve this wavelength from the carbon K line. Using the target cleaning procedures described in the preceding section, however, on all other targets, we routinely detect traces of carbon ranging from 0.5 to 2 μg/cm^2 resulting from the cleaning process. These carbon traces are only eliminated by the usual reduction procedures using oxygen and hydrogen gas with the target at elevated temperatures. Since 2 μg/cm^2 of carbon results in an x-ray yield of 1.06×10^{-5} photons/proton for 100-keV incident protons, we feel that the trace amounts of carbon would contribute less than 5% to our measured Rh M-shell yields.

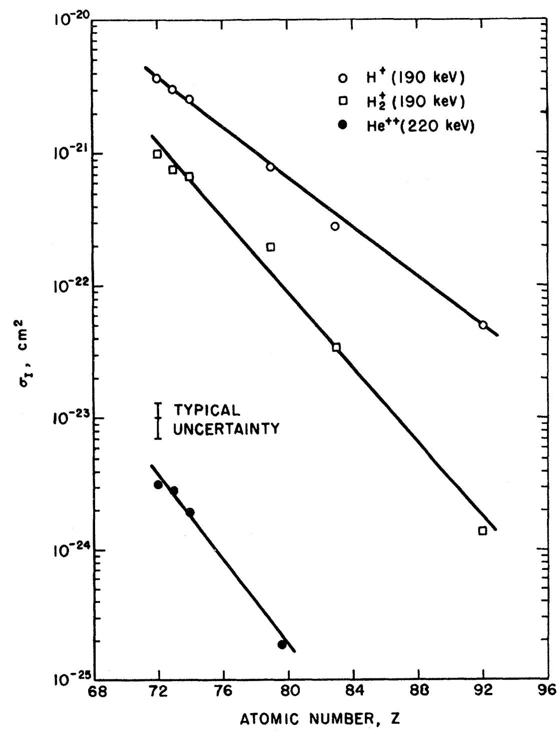

FIG. 6. Comparison of the Z dependence of the M-shell ionization cross sections for 190-keV H^+, 190-keV H_2^+, and 220-keV He^{++} ions.

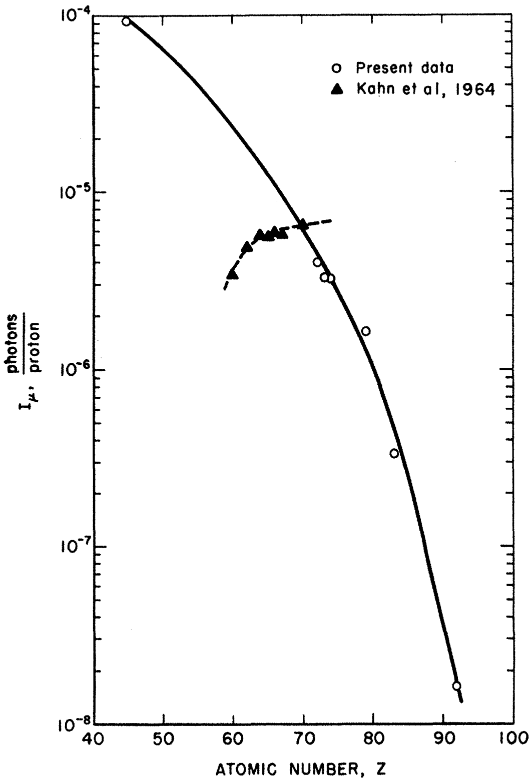

FIG. 7. X-ray production efficiencies I_μ (photons/proton) from the present experiment as a function of target atomic number Z. Also included are earlier values published by Khan *et al.* The systematics of the two sets of values for the I_μ exhibit sharply different Z dependences.

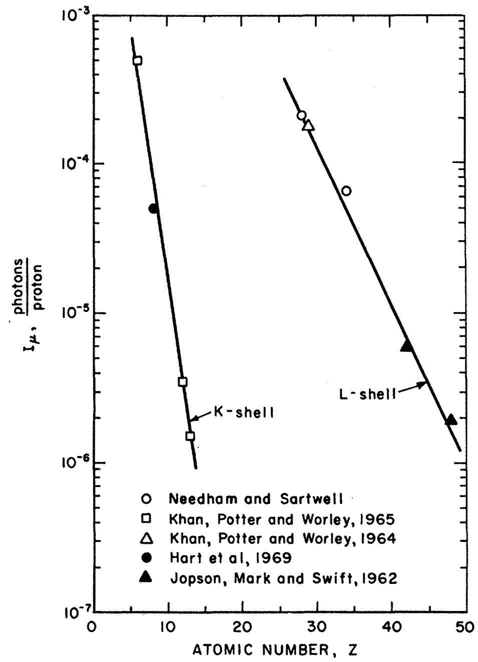

FIG. 8. Proton-excited K- and L-shell x-ray yields I_μ as a function of the target atomic number Z. The increase in the x-ray yield with increasing wavelengths characteristic of lower-Z materials has been clearly established in recent years.

Earlier data for the K and L shells are available which can be plotted as I_μ versus Z.[2–5] The Z dependence for proton-excited K- and L-shell x-ray yields shown in Fig. 8 displays the same general functional dependence as our present M-shell yields.

CONCLUSION

We have performed a systematic experimental study of the excitation of M-shell x rays from atoms with $72 \leq Z \leq 92$. No attempt was made to relate the experimentally determined ionization cross sections to theoretical values. However, work is currently being performed at this laboratory using the Bethe-Born form factors for the M subshells, as developed by Khandelwal and Merzbacher,[19,20] for application to our present experimental results, as well as to an extension of this study down to targets of $Z = 40$.

The Z dependences of the ionization cross sections presented here are consistent with the systematics obtained previously for ion excitation of the atomic K and L shells.

The large spread in the possible transitions to the various M subshells reduces some of the measured x-ray yields in relation to the actual M-shell ionization process. This results from the use of nondispersive x-ray detection techniques. Recently, however, a crystal x-ray spectrometer system was installed, and we will shortly begin measurements in which the full emission spectra in the M shells will be obtained by using ion excitation.

ACKNOWLEDGMENTS

The authors thank W. Lederer for the design and construction of much of the experimental equipment and operation of the ultrahigh-vacuum systems. We would also like to thank S. Arkin for his assistance in operation of the accelerator, and W. Bateman for his help in the preparation of this manuscript.

[1]H. W. Lewis, B. E. Simmons, and E. Merzbacher, Phys. Rev. 91, 943 (1953).

[2]E. M. Bernstein and H. W. Lewis, Phys. Rev. 95, 83 (1954).

[3]S. Messelt, Nucl. Phys. 5, 435 (1958).

[4]R. C. Jopson, Hans Mark, and C. D. Swift, Phys. Rev. 127, 1612 (1962).

[5]J. M. Khan and D. L. Potter, Phys. Rev. 133, A890 (1964); J. M. Khan, D. L. Potter, and R. D. Worley, *ibid.*, 134, A316 (1964); 135, A511 (1964); 136, A108 (1964); 139, A1735 (1965); 145, 23 (1966).

[6]W. Brandt, R. Laubert, and I. Sellin, Phys. Rev.

151, 56 (1966).
[7]W. Henneberg, Z. Physik 86, 592 (1933).
[8]T. Huus, J. H. Bjerregaard, and B. Albek, Kgl. Danske Videnskab. Selskab, Mat. Fys. Medd. 30, No. 17 (1956).
[9]E. Merzbacher and H. W. Lewis, *Encyclopedia of Physics*, edited by S. Flügge (Springer-Verlag, Berlin, 1958), Vol. 34, p. 166.
[10]D. Jamnik and C. Zupancic, Kgl. Danske Videnskab. Selskab, Mat. Fys. Medd. 31, No. 2 (1957).
[11]J. Bang and J. M. Hansteen, Kgl. Danske Videnskab. Selskab, Mat. Fys. Medd. 31, No. 13 (1959).
[12]W. Brandt and R. Laubert, Phys. Rev. 178, 225 (1968).
[13]K. D. Champion, H. J. Hurst, and R. N. Whittem, Lucas Heights Report No. AAEC-TM 454 (1968) (unpublished).
[14]R. W. Fink, R. C. Jopson, H. Mark, and C. D. Swift, Rev. Mod. Phys. 38, 513 (1966).
[15]S. D. Warshaw and S. K. Allison, Rev. Mod. Phys. 25, 779 (1953).
[16]L. C. Northcliffe, Ann. Rev. Nucl. Sci. 13, 67 (1963).
[17]P. G. Steward and R. Wallace, UCRL Report No.-17314, 1966 (unpublished).
[18]J. M. Khan, D. L. Potter, and R. D. Worley, Phys. Rev. 135, A511 (1964).
[19]G. S. Khandelwal and E. Merzbacher, Phys. Rev. 144, 349 (1966).
[20]G. S. Khandelwal and E. Merzbacher, Phys. Rev. 151, 12 (1966).

PHYSICAL REVIEW A VOLUME 2, NUMBER 5 NOVEMBER 1970

Hyperfine Structure of $^5I_{8,7}$ Atomic States of $Dy^{161,163}$ and the Ground-State Nuclear Moments*

W. J. Childs
Argonne National Laboratory, Argonne, Illinois 60439
(Received 23 April 1970)

The atomic-beam magnetic-resonance technique has been used to measure the hyperfine structure of the $4f^{10}6s^2\,{}^5I_{8,7}$ atomic states of $Dy^{161,163}$. Values of the hyperfine-interaction constants A, B, and C, corrected for hyperfine interactions with other states, are given for both atomic states of each isotope. It is found that for the nuclear ground states of $Dy^{161,163}$, $\mu^{163}/\mu^{161} = -1.400(3)$, and, less accurately, $\mu^{163} = +0.65(6)\mu_N$, $Q^{163} = +2.51(30)$ b, $\mu^{161} = -0.46(5)\mu_N$, $Q^{161} = +2.37(28)$ b. The electron g factor g_J is measured for the atomic states $4f^{10}6s^2\,{}^5I_{8,7,6}$ and also for the lowest $J=8$ level of $4f^9 5d6s^2$ at 7565 cm^{-1}. The lifetime of this level cannot be appreciably less than 2 msec, the transit time for the atom in the apparatus.

I. INTRODUCTION

Ebenhoh, Ehlers, and Ferch[1] pointed out that the electric-quadrupole moment of the Dy^{161} nuclear ground state appeared about 50% larger when determined from the Mössbauer effect[2] than from paramagnetic resonance in salts[3] (presumably because of difficulties in estimating the electric field gradient at the nucleus). Their atomic-beam magnetic-resonance value, obtained with free atoms, confirmed the Mössbauer result.

The purpose of the present experiment was to extend the atomic-beam experiment[1] on the $4f^{10}6s^2\,{}^5I_8$ atomic ground state of Dy^{161} and Dy^{163} to include measurements of the $\Delta F = \pm 1$ hfs intervals, and to make corresponding measurements on the $^5I_7$ metastable state. When hfs measurements are made in only one atomic state, one must postulate details of the state in order to extract values for the magnetic-dipole and electric-quadrupole moments of the nuclear ground state from the observed hfs. As more atomic states are included in the hfs studies, the assumptions about the atomic state become subject to test.

In determining values of the magnetic-dipole moments of the $Dy^{161,163}$ nuclear ground states, it is shown that atomic core polarization is responsible for only about 1% of the magnetic-dipole hfs. The effects of relativity and the intermediate-coupling composition of the $^5I_{8,7}$ states are taken into account explicitly, and Sternheimer's estimate of the distortion of the inner electron shells is included in extraction of the nuclear electric-quadrupole moment.

Precision values of the electron g factor g_J are also useful in understanding the composition of atomic states and were therefore determined for all states having sufficient population in the atomic beam.

II. EXPERIMENTAL CONSIDERATIONS

The principles of the atomic-beam magnetic-resonance technique have been discussed[4] many times in the literature, as has the particular apparatus used for the present experiment.[5] The latter is entirely conventional except that the digital techniques used[6] for handling the data made possible observation of transitions in very weakly populated atomic